Isotopic shifts in vibration levels of ozone due to homogeneous substitution: Band centres of 18O3 derived from analysis of CW-CRDS spectra in the 5900-7000 cm-1 range

Eugenia N. Starikova, Alain Barbe, Marie-Renée de Backer, Vladimir G. Tyuterev, S. A. Tashkun, S. Kassi, A. Campargue

Isotopic shifts in vibration levels of ozone due to homogeneous substitution: band centres of $^{18}O_3$ derived from analysis of CW-CRDS spectra in the 5900-7000 cm^{-1} range

E.N. STARIKOVA[1,2], A. BARBE[1], M.-R. DE BACKER-BARILLY[1],

Vl.G. TYUTEREV[1], S.A. TASHKUN[2], S. KASSI[3], A. CAMPARGUE[3]

[1] *GSMA, UMR CNRS 6089, UFR Sciences Exactes et Naturelles, BP 1039, 51687 Reims Cedex 2, France.*

[2] *Laboratory of Theoretical Spectroscopy, Institute of Atmospheric Optics, Russian Academy of Sciences, 1, av. Akademicheskii, Tomsk 634055, Russia.*

[3] *Laboratoire de Spectrométrie Physique, UMR CNRS 5588, Université Joseph Fourier, BP 87, 38402 Saint Martin d'Hères, France.*

Corresponding author: vladimir.tyuterev@univ-reims.fr

Abstract

More than 5050 rovibrational transitions were assigned in the very sensitive CW-CRDS $^{18}O_3$ spectra in the 5900 – 7000 cm^{-1} range leading to the first determination of 14 new vibrational band centres. Three bands correspond to the highest ozone states observed so far under high resolution. The good agreement between predicted and observed centres (*rms* deviation of 1.1 cm^{-1}) confirms the accuracy of the potential function previously determined from $^{16}O_3$ data. At this energy range situated ~ 20% below the dissociation energy, the small changes of masses associated with the $^{16}O_3 \rightarrow {}^{18}O_3$ homogeneous isotopic substitution result in irregular isotopic shifts.

1. Introduction

Despite considerable effort from the scientific community devoted to the investigation of ozone properties and spectra, there remain many issues and puzzling problems which are far from being completely solved, like, for example, the interpretation of anomalous isotopic enrichment effect in the ozone formation [1-3], the calculation of the dissociation and recombination rates [4-5], a detailed description of non-local thermodynamic equilibrium processes in the upper atmosphere [6], or the search of optimal channels for multi-photon laser excitation of ozone. A solution for many of these problems requires detailed information on high-energy rovibrational states of the ozone isotopic species. Accurate measurements and calculations of these states in the energy range approaching the dissociation limit are a particular challenging issue.

The high-resolution spectroscopy of ozone has a long history. Up to 5800 cm^{-1} the infrared spectra have been mostly obtained by FTS (Fourier Transform Spectroscopy). The range of fundamental and first overtone and combination bands of the principal isotopologue, $^{16}O_3$, has been covered in series of studies by Flaud, Camy-Peyret et al. [7-9] resulting in an atlas of line parameters up to 3000 cm^{-1} [9]. Barbe et al. [10-13] have extended the range of observations assigning more than 30 bands of $^{16}O_3$ up to 5800 cm^{-1}. Ozone spectroscopy studies available up to 2003 have been reviewed by Steinfeld et al. [14], Flaud and Bacis [15], Mikhailenko et al. [16], and Rinsland et al. [17].

FTS spectra of ozone enriched in ^{18}O and ^{17}O were analysed in Refs. [15,18-26]. The most extended spectral regions were investigated by Chichery et al. [21,22] for the homogeneous isotopic variant $^{18}O_3$ and by De Backer, Barbe et al. [23-26] for the mixed variants $^{16}O^{18}O^{16}O$, $^{18}O^{16}O^{18}O$, $^{16}O^{16}O^{18}O$ and $^{16}O^{18}O^{18}O$. All previously available studies of isotopically substituted ozone spectra were performed below 4900 cm^{-1} and involved bands having at maximum a $\Delta\boldsymbol{\nu} \equiv \sum_i \left|\Delta\boldsymbol{\nu}_i\right| = 5$ variation of the vibration quantum numbers. A large part of the related results are available in the S&MPO (Spectroscopy & Molecular Properties of Ozone) information system [27], which is accessible *via* the websites ozone.univ-reims.fr and ozone.iao.ru.

There are two major problems in deriving information about the vibration levels of ozone approaching the dissociation limit (situated near 8500 cm^{-1} [15]) from high-resolution absorption spectra. One is experimental: band strengths are quickly decreasing with the vibrational excitation, and a higher sensitivity than that provided by FTS is necessary: up to eight orders of magnitude are noted between the band strength of the ν_3 fundamental and that

of the bands near 7000 cm^{-1} corresponding to $\Delta\omega = 8$. The other problem is related to an increasing complexity of analyses due to many accidental vibration-rotation resonance perturbations and missing information on "dark" states.

A breakthrough in the extension of experimental measurements to higher energy has been achieved with the development of very sensitive laser techniques [28-34]. Wentz et al. [28] measured more than 3500 lines in the $^{16}O_3$ spectrum recorded with a tunable single mode diode laser between 6430 and 6670 cm^{-1} but only about 400 of them could be assigned. A further progress has been achieved with the CW-Cavity Ring Down Spectrometer (CW-CRDS) developed at Grenoble University [34] in the wide 5850-7000 cm^{-1} region [29-34], where more than 7500 lines of $^{16}O_3$ have been recently recorded and assigned in collaboration with the Reims group. These results have been recently reviewed by Campargue et al. [34].

On the theoretical side, considerable efforts have been devoted to the determination of the potential energy surface (PES) [5, 35-41 and references therein], for the electronic ground state of ozone. Extended *ab initio* calculations have been performed by Siebert and Schinke et al. [36,37]. Babikov et al. [38] and Grebenshchikov et al. [39] used these calculations to study the metastable states and the van der Waals states, respectively. Related dynamical studies have been summarized and reviewed in Ref. [5]. Up to date, the most accurate empirical PES for the spectroscopic calculations at the open configuration have been determined by Tyuterev et al. [40, 41] from the fit of FTS experimental vibration-rotation data of $^{16}O_3$ below 5800 cm^{-1}. This PES has been used, for a theoretical interpretation of rates of formation of ozone isotopologues [3], for the assignment of CW-CRDS spectra of $^{16}O_3$ [29-34] and for the extrapolation towards highly excited vibrational states [35].

In this Letter, we report the first results of experimental and theoretical studies of the isotopic effect in high-resolution spectra of the ozone molecule due to the $^{16}O_3 \rightarrow {}^{18}O_3$ substitution in the 5900 – 7000 cm^{-1} wavenumber range. Ro-vibrational levels corresponding to the high energy edge of this range are at about 82% of the dissociation limit. Contrary to the low energy range, the isotopic shifts of the band centres appear to be irregular even though the change in masses is small and homogeneous. This reflects the complexity of anharmonic interactions in the ozone molecule. Due to the shifts of about 340 cm^{-1} towards lower wavenumbers for the band centres with respect to the major isotopologue, we were able to record three $^{18}O_3$ new bands which correspond to the largest vibrational excitation ever detected in ozone spectra at high resolution. One of the goals of this study was to use these new observations to check to what extent the PES of Refs. [40, 41] determined from $^{16}O_3$ data, is valid for accurate predictions of the $^{18}O_3$ bands.

In Section 2, theoretical calculations of energy levels and wave functions relevant to the observed bands are briefly described; Section 3 is devoted to the experimental set up and recorded spectra; Section 4 to the spectral analysis and Section 5 to the discussion of the obtained results.

2. Band centres predicted from PES

At low vibrational excitation, the assignment of ozone bands has been traditionally based on Dunham-type expansions involving Darling-Dennison resonance terms which couple stretching vibrations due to the proximity of the ω_1 and ω_3 harmonic frequencies [15, 16]. This simple approach is no more valid at higher energies because of the increasing density of states and of the overlapping of stretching polyads defined by the condition $\upsilon_1 + \upsilon_3 = const$ [11-13, 16, 21-34]. The overlapping of the polyads results in numerous unusual resonances corresponding to large differences in vibrational quantum numbers up to $\Delta\upsilon = 10$.

In previous analysis of the CW-CRDS spectra of $^{16}O_3$ [29-34], our assignments relied on extrapolations from the empirical PES of Refs. [40, 41]. For the 21 band centres of $^{16}O_3$ reported in the 5850-7000 cm^{-1} range, the deviations of the predictions from observations vary from 0.1 to 2.4 cm^{-1} with a *rms* error of about 1 cm^{-1}. For the vibrational assignments of the present $^{18}O_3$ spectra, we used two versions of the same PES, one adapted to the Morse-cosine kinetic model [40], another adapted to the exact kinetic energy operator [41]. The corresponding calculations using both versions of the PES result in energies for $J = 0$ and $J = 1$ levels which are in a good agreement at least up to 7000 cm^{-1} (see Table 1): the *rms* deviation between two calculations is 0.9 cm^{-1}.

As far as techniques of calculations are concerned, two complementary and completely independent methods were applied. The first method uses variational calculations involving numerical integration in a large basis set of primitive wave functions defined in internal bond length and bond angle or Radau coordinates, as described in Refs. [40, 41]. In order to achieve a convergence of calculations in the considered energy region, it was necessary to extend the size of the basis by at least one order of magnitude compared to similar calculations for water molecule (see Ref. [41] for the corresponding discussion). The second method is purely algebraic and uses successive high-order Contact Transformations (CT) of the complete vibration-rotation Hamiltonian into series of effective Hamiltonians defined for groups of strongly interacting vibrational states. In our analysis, the MOL_CT suite of computational

codes [42] was used to allow for a systematical building of effective Hamiltonians in normal coordinates [42, 43]. These calculations account for various resonance interactions specific to the ozone molecule including inter-polyad couplings. This method has the advantage to directly provide with the expansion of eigen-functions $|\Psi_{\Gamma N_V}>$ of the final transformed Hamiltonian in the normal mode basis:

$$|\Psi_{\Gamma N_V}>=\sum_{v_1v_2v_3} C^{\Gamma N_V}_{v_1v_2v_3}\,|v_1v_2v_3>_0 \qquad (1)$$

Here Γ is the symmetry type of the state and N_V is the rank number of the vibration state according to the increasing energy for a given Γ. The normal mode basis $|v_1v_2v_3>_0=|v_1>_0|v_2>_0|v_3>_0$ corresponds to vibrations which are decoupled near the minimum of the potential well. Eq. (1) stands for vibration wave functions. Similar expansions are also obtained for vibration-rotation wave functions involving asymmetric top rotational basis $|JK_aK_c>$ as a direct product in the right hand side of Eq.(1). This offers a rigorous procedure for normal mode spectroscopic assignments of ro-vibrational states from a given PES.

The mixing coefficients are defined as squares of the expansion coefficients:

$$P_n=(C^{\Gamma N_V}_{v_1v_2v_3})^2 \text{ with } \sum_n P_n=1 \qquad (2)$$

Here n = 1 corresponds to the largest contribution in Eq. (1) and the terms with n = 2, 3, … correspond to the decreasing order of the mixing coefficients. The convergence of MOL_CT algebraic calculations with increasing orders of CT was checked against variational calculations with the same PES. For the $^{16}O_3$ and the $^{18}O_3$ vibration levels, the *rms* deviation between these two calculations up to 7000 cm^{-1} are less than one wavenumber for the 8th order of contact transformations. For this reason, only CT calculations ("calc_2") corresponding to the PES of [41] are provided in Table 1.

In this work, we use two types of vibration state identification. The first one is the (Γ, N_V) global assignment containing the symmetry species Γ (=A_1 or B_1) and the ranking number N_V only. If a PES is sufficiently accurate *i.e.* (obs.-calc.) errors are much smaller than the energy separation, this global assignment is *unambiguous.* Further comparisons with observations clearly show that this is our case: there is no ambiguity in the global (Γ, N_V) assignment in the considered spectral range. Between 5900 and 7000 cm^{-1}, both PES [40, 41]

result in 28 calculated ($B_1 \leftarrow A_1$) *A*-type bands due to the dipole moment component parallel to the "linearization" *z*-axis and in 33 calculated ($A_1 \leftarrow A_1$) *B*-type bands due to the dipole moment component perpendicular to the "linearization" *z*-axis. Symmetry labels correspond to the standard choice of axes for the open configuration of the ozone molecule as described in [9, 15]. The second type of assignment is the traditional normal mode assignment relying on $\upsilon_1\upsilon_2\upsilon_3$ labels corresponding to the major normal mode contribution in the expansion (1).

According to the nuclear spin statistics only ro-vibrational levels of A_1 and A_2 symmetry types are allowed in the case of $^{16}O_3$ and $^{18}O_3$ [9, 15]. This means that the lowest allowed levels correspond to $\{(\upsilon_1)(\upsilon_2)(\upsilon_3)_{even}[JK_aK_c = 000]\}_{A_1}$ for A_1 type vibrations and to $\{(\upsilon_1)(\upsilon_2)(\upsilon_3)_{odd}[JK_aK_c = 101]\}_{A_2}$ for B_1 type vibrations. Predictions for these lowest allowed levels corresponding to the bands observed in this work are given in Table 1 together with their three major mixing coefficients P_n associated with normal mode contributions $W_n = |\upsilon_1\upsilon_2\upsilon_3>_0$ for n =1, 2, 3.

3. Experiment

For this work, the CW-CRDS spectra of $^{18}O_3$ were recorded with the same CW-CRDS spectrometer as used in our previous studies of the main ozone isotopologue [29-34] and of other species of atmospheric importance such as H_2O [45, 46] and $^{12}CO_2$ [47, 48]. The detailed description of the fibered set up can be found in Refs. [29, 44, 48]. Briefly, the full 5900-7000 cm^{-1} range was covered with a set of about 50 Distributed Feed-Back (DFB) laser diodes. The tuning range of each DFB laser is about 7 nm (~ 30 cm^{-1}) for a temperature variation from -10 to 65°C. The typical sensitivity (noise equivalent absorption α_{min}~2-5×10^{-10} cm^{-1}), the wide spectral coverage and the four to five decades linear dynamic range make this CW-CRDS spectrometer an ideal tool for high sensitivity absorption spectroscopy in the important atmospheric window of transparency around 1.5 μm. The typical ring down times are on the order of 60 μs. A few hundreds ring down events are averaged for each spectral data point, and the duration of a temperature scan is about 70 minutes for each DFB laser. The pressure, measured by a capacitance gauge, as well as the ring down cell temperature, was monitored during the spectrum acquisition. Note that the DFB line width is much smaller than the Doppler broadening (about 10×10^{-3} cm^{-1} (FWHM) at 6000 cm^{-1}), so that the observed resolution is mostly Doppler limited since the pressure broadening is about 5×10^{-3} cm^{-1} (FWHM) at a typical pressure of 20 Torr.

The 140 cm long CRDS cell fitted by the super mirrors was filled with a typical pressure of 30 Torr of ^{18}O enriched oxygen. The quasi complete conversion of oxygen in ozone (P = 20 Torr) was obtained after a few minutes with a silent electric discharge (12 kV, 400 Hz). The ^{18}O enrichment of the molecular oxygen used for the ozone synthesis was 95 %, leading to an 86 % partial pressure of the $^{18}O_3$ homogeneous isotopologue. Consequently, the other minor isotopic species - mainly $^{16}O^{18}O^{18}O$ and $^{18}O^{16}O^{18}O$ - contributed to the absorption spectra through many weak absorption lines superimposed on the $^{18}O_3$ spectrum. The spectrum analysis was further complicated by the presence of absorption lines of several impurities which were generally ^{18}O enriched: $H_2{}^{18}O$ (and $H_2{}^{16}O$), $^{12}C^{18}O$, $^{16}O^{12}C^{18}O$ or $^{12}C^{18}O_2$. The $H_2{}^{18}O$, $^{16}O^{12}C^{18}O$ and $^{12}C^{18}O$ transitions were identified on the basis of the HITRAN database [49] and of our recent CW-CRDS investigation of the CO_2 spectrum [48].

The wavenumber calibration of the spectrum is based on the wavelength values measured by a wavemeter (Burleigh WA1640) during the DFB frequency scan. When necessary, it is further refined by simply stretching the frequency scale (with an origin at 0) in agreement with highly accurate positions of reference lines due to impurities. $H_2{}^{18}O$ and $H_2{}^{16}O$ line positions as provided by the HITRAN database [49] were used as reference lines. The obtained absolute wavenumber calibration is estimated accurate within 2×10^{-3} cm^{-1}.

The entire spectrum range of our recordings with band assignments and impurity absorption features is shown in Fig 1.

4. Band centres determined from the rovibrational analysis of the CRDS spectra

Among triatomic atmospheric molecules, the ozone molecule is a relatively heavy one with dense rotational structure. In the case of an absorption band at room temperature, depending on the band type, the most intense lines correspond to J values in the 15-35 range. As seen in Table 1, most of the bands falling in our spectral region correspond to 7 or 8 vibration quanta of the excited state. These bands are extremely weak and a complete set of transitions from low-populated levels with small J values could not be detected for some of them, even with the achieved CW-CRDS sensitivity. This makes difficult an experimental determination of the band centres.

The centre of a rovibrational band is defined as the $J \rightarrow 0$ extrapolation of the upper state energies. This $J \rightarrow 0$ limit could be accurately determined by following line series in P, Q or R branches in a sufficiently large range of J, K_a values. This implied the full rovibrational assignment of the recorded spectrum. As illustrated in our previous analysis of the CW-CRDS spectrum of $^{16}O_3$ case [29-34], the assignment and modelling of the thousands of $^{18}O_3$ lines

observed between 5900 and 7000 cm^{-1} represents a considerable task. The very large number of possible rovibrational resonance interactions, in particular with dark states, made an accurate modelling in the frame of the effective Hamiltonian, very difficult. The obtained spectra, displayed in Fig. 1, were divided in five spectral intervals corresponding to interacting bands systems which could be treated independently: 5930-6080, 6170-6280, 6320-6400, 6490-6650 and 6745-6840 cm^{-1}. Conceptually, the assignment procedure had many features in common with those encountered for $^{16}O_3$ spectra [29-34]. However as a consequence of the irregular behaviour of the isotopic shifts (see below), the resonance situation is in fact quite different. The detailed presentation of these analyses and of the derivation of the rotational, centrifugal distortion and resonance coupling parameters is beyond the scope of this letter and will be published separately. As an illustration of the achieved results, we include in Table 2 the total number of transitions assigned for the different bands. Here, we limit our discussion to the derivation of the band centre with the best possible accuracy.

The simultaneous modelling of the bands belonging to coupled band systems made it possible to identify the levels perturbed by resonance interactions. The line series remaining after the exclusion of these strongly perturbed levels were fitted using an isolated band model i.e. by using the standard Watson rotational Hamiltonian. The band centre was then obtained through the $J \rightarrow 0$ extrapolation. For most of the bands a sufficient accuracy of the band centre was achieved using line series truncated at J and K_a maximum values of 20 and 4, respectively. In the case of the $\nu_1+3\nu_2+4\nu_3$ band, rovibrational lines up to $J = 30$ have been included into the fit because the number of lines observed for $J \leq 20$ was too limited to achieve a sufficient accuracy on the band centre determination. The obtained band centres are listed in Table 2 with their respective accuracy taken as the *rms* deviation between the truncated (see above) sets of observed and calculated line positions for each considered band. The uncertainty for all observed retrieved band centres is smaller than 3×10^{-2} cm^{-1} which is largely sufficient in comparison with the isotopic shifts which are observed to vary between 296 and 372 cm^{-1} in our range.

Once the experimental value of the band centre was obtained, the global (Γ, N_V) vibrational assignment was rather straightforward relying on the good agreement between predicted and experimentally determined band centres (Table 2). (The *rms* value of the deviations is 1.1 cm^{-1}). The situation is more complicated for the normal mode assignment. As stated in previous works about $^{16}O_3$ [29-34, 40], a normal mode labelling becomes ambiguous for some high vibration states above half the dissociation energy. The main reason is a strong

mixing of the basis wavefunctions due to various anharmonic interactions. Table 1 shows that for many bands no normal mode contribution is truly dominant. In addition to the global (Γ, N_V) assignment, we provide in Table 1 the normal mode vibrational quantum numbers $(\alpha_1,\alpha_2,\alpha_3)$ corresponding to the major contributions in Eq. (1). Since for small values of the J rotational quantum numbers, the normal mode mixing coefficients remain nearly unchanged, we use the decomposition given in Table 1 for the normal mode assignment of the observed bands. Labelling the vibrational bands with the dominant $(\alpha_1,\alpha_2,\alpha_3)$ state follows the spectroscopic tradition of ozone studies, but one should keep in mind that these "nominative" notations may be ambiguous at high energy range: for instance, the two bands at 6392 and 6643 cm^{-1} correspond to upper states having the same principal normal mode contribution (see Table 1). However the knowledge of the normal mode mixture is of great help for a better understanding of possible resonance interactions.

Note that the local mode labeling [50] does not provide a satisfactory alternative in a sufficiently wide frequency range for the ozone vibrations either [40], because strong interactions with the bending mode break down the pure stretching model for the normal-to-local mode transitions.

5. Discussion: isotopic effect on band centres and assignments

Fig. 2 shows a comparison of the simulated spectra using assigned rovibrational lines for $^{18}O_3$ (upper panel) and $^{16}O_3$ (lower panel) in the region of the $5\nu_1+\nu_3$ band as obtained in this work and in Ref. [33], respectively. On average, the $^{18}O_3$ bands lie at about 340 cm^{-1} below the corresponding $^{16}O_3$ bands, but it is clear that individual isotopic shifts are not regular. For instance, the overlapping between the $5\nu_1+\nu_3$ and $2\nu_2+5\nu_3$ bands is quite different for the two isotopologues.

Irregular variations of isotopic shifts due to isotopic substitutions have been observed for other molecules, however contrary to these previous studies the $^{16}O_3 \rightarrow {}^{18}O_3$ substitution is *homogeneous* that makes this situation rather unique. Indeed, usually an isotopic substitutions change the forms of mass dependent normal vibrations probing then different directions onto the molecular PES. In our case the comparison of **L** matrices which link internal and normal coordinates makes it obvious that they are exactly proportional. The ratio of matrix elements $\mathbf{L}_{nm}$ (666) / $\mathbf{L}_{nm}$ (888) = 1.0300 is the same in all significant digits. Consequently the forms of normal mode vibrations are identical for $^{16}O_3$ and $^{18}O_3$. Also the relative mass changes are very small. In these conditions, if one assumes that ozone normal modes form regular stretching

Darling-Dennison (DD) polyad sequences (due to the $\omega_1 \approx \omega_3$ resonance), these polyad structures have to be very similar for both isotopic species and consequently the isotopic shift would be regular as well. This is not what we observe in our energy range.

Isotopic substitutions modify importantly the effect of resonance interactions leading, in some cases, to different vibrational mixing and then different vibrational labelling as illustrated by the highest frequency bands of Fig 2. Note that upper states of these two bands have the same global assignment 46B but the normal mode assignments belong to different stretching polyads: $(\upsilon_1 + \upsilon_3 = 5, \upsilon_2 = 2)$ for $^{16}O_3$ and $(\upsilon_1 + \upsilon_3 = 6, \upsilon_2 = 1)$ for $^{18}O_3$. In terms of normal modes these are mixed states (Tables 1 and [33]) with the extra-polyad contributions different for $^{16}O_3$ and $^{18}O_3$. Extra-polyad interactions responsible for this re-assignment depend on accidental coincidences of polyad patterns corresponding to different υ_2 values. This suggests that such interactions localised in narrow energy intervals and distributed in an irregular way are very sensitive to mass changes even though the latter are small and homogeneous. In order to verify this suggestion we have proceeded with the following test: band centres were calculated via the vibrational extrapolation by the polyad effective Hamiltonian model following increasing values of $P = \upsilon_1 + \upsilon_3$. This simplified DD model contains all intra-polyad coupling terms $< \upsilon_1 \pm 2 | H^{eff} | \upsilon_3 \mp 2 >$, $< \upsilon_1 \pm 4 | H^{eff} | \upsilon_3 \mp 4 >$, …accounting for the Darling-Dennisson $\omega_1 \approx \omega_3$ resonance but excludes all extra-polyad couplings terms. The computed band centre for the 45B←1A band (in the middle of Fig 2) was in excellent agreement with our full calculations and with experiment for both isotopologues: the error < 1 cm^{-1}. This is consistent with the normal mode decomposition of Table 1, which does not contain extra-polyad contributions for the 45B state. But the situation is quite different for other two bands of Fig 2. For the right hand side 46B←1A band, the DD polyad model gave the same normal mode assignment $\nu_1 + \nu_2 + 5\nu_3$ for both isotopologues contrary to full calculations (Tables 1,2 and [ ]), the error being -20 cm^{-1} for $^{16}O_3$ and -10 cm^{-1} for $^{18}O_3$. For the left hand side 44B←1A band, the DD polyad model gave the error with the opposite sign: +17 cm^{-1} for $^{16}O_3$ and +8 cm^{-1} for $^{18}O_3$. For both bands the test result is consistent with the normal mode decomposition of wave functions (Table 1 and [33]), because the extrapolyad contributions are larger for $^{16}O_3$ than for $^{18}O_3$. This means that accidental exptrapolyad normal more couplings contribute to the isotopic shift in a rather irregular manner.

Fig. 3 represents the energy dependence of the isotopic shift in two ways:

i) in the upper panel, we plotted the difference of the $^{16}O_3$ and $^{18}O_3$ band centres corresponding to the same (Γ, N_V) global assignment. All observed $^{18}O_3$ bands given in Table 2 were included in this comparison. The filled symbols stand for the partner bands of the $^{16}O_3$ isotopologue which were directly observed in Refs. [29-34], the grey-filled symbols correspond to the $^{16}O_3$ values which were determined *via* "dark" state resonance perturbations as described in Refs. [29-34], open symbols correspond to the bands which have not yet been observed in $^{16}O_3$ spectra. In the latter case, we used calculated positions for $^{16}O_3$ which proved to be sufficiently accurate at the scale of the Figure.

ii) in the lower panel of Fig. 3, the comparison of the band centres is based on the normal mode assignments which are traditionally employed in ozone spectroscopy: we associated the bands of $^{16}O_3$ and $^{18}O_3$ for which the upper states correspond to the most similar normal mode mixtures. As stated before, this procedure leads to ambiguities in some cases because the resonance situations change quite substantially from one isotopologue to the other. This is clearly observed in Fig. 4, where the first expansion coefficients for the partner bands of $^{16}O_3$ and $^{18}O_3$ are plotted. Certain correlations are noted between the irregular variation of P_1 (Fig. 4) and that of the isotopic shifts (Fig 3).

In conclusion, fourteen new band centres of $^{18}O_3$ were determined from high-sensitive CRDS observations. The *rms* deviation of theoretical predictions from observed band centres is 1.1 cm^{-1} confirming the validity of the empirical PES of Refs. [40, 41] for this isotopologue. In particular, the three highest ozone bands observed so far at high resolution with upper states (Γ, N_V) = (A_1, 82), (B_1, 64), (B_1, 66), which were beyond the accessible range for $^{16}O_3$, are also in a good agreement with calculations.

Previous studies of $^{18}O_3$ spectra [15, 19, 21, 22] below 5000 cm^{-1} suggested that isotopic shifts varied smoothly according to the simple relation for harmonic vibration frequencies, $\omega^* / \omega \sim \sqrt{m / m^*}$, allowing for a direct transfer of the vibrational labelling to the partner bands. This is no more valid in our spectral range reaching 82% of the ozone dissociation energy. The variation of the isotopic shifts still depends on normal mode quantum numbers $(\boldsymbol{v_1}, \boldsymbol{v_2}, \boldsymbol{v_3})$ but appears to be more irregular as a consequence of drastic changes in the resonance interactions pattern and in the normal mode composition of the considered states. As discussed above, the extrapolyad interactions play an important role in such behaviour. This work gives thus an experimental evidence for the strong mixing of the normal modes vibrations for some ozone states in the 6000-7000 cm^{-1} range. The coupling of normal modes

should also have a considerable impact on the probabilities for dipole excitation channels in this high energy range.

Very few molecules allow studying effects of homogeneous isotopic substitutions, and to our knowledge for none of them a sufficiently large set of experimental data on high-energy vibrations was yet available. A further step of this study will be to determine a full set of accurate rotational constants, centrifugal distortion, dipole moment transition and resonance coupling parameters as well as "dark" state perturbations for all bands involved in order to produce a synthetic spectrum. In addition, we plan to study the isotopic effects on the spectrum of the non-homogeneously substituted species ($^{16}O^{18}O^{16}O$, $^{18}O^{16}O^{18}O$, $^{16}O^{16}O^{18}O$, and $^{16}O^{18}O^{18}O$) for which even stronger changes are expected.

Acknowledgements

We acknowledge the support from a collaborative program between CNRS-France and RFBR-Russia (PICS grant No 05-05-22001). We are grateful to S.Mikhailenko for stimulating discussions. The support from IDRIS computer centre of CNRS France and Champagne-Ardennes regional computer centre for global calculations is also acknowledged.

References

[1] Y.Q. Gao, R.A. Marcus, Science 293 (2001) 259.
[2] Ch. Janssen, J. Guenther, K. Mauersberger, D. Krankowsky, Phys. Chem. Chem. Phys. 3 (2001) 4718.
[3] A. Miklavc, S.D. Peyerimhoff, Chem. Phys. Lett. 359 (2002) 55.
[4] R. Hernandez-Lamoneda, M.R. Salazar, R.T Pack, Chem. Phys. Lett. 355 (2002) 478.
[5] R. Schinke, S.Yu. Grebenshchikov, M.V. Ivanov, P. Fleurat-Lessard, Annu. Rev. Phys. Chem. 57 (2006) 625.
[6] M. Lopez-Puertas, B. Funke, S. Gil-Lopez, M.A. Lopez-Valverde, Thomas von Clarmann, H. Fischer, H. Oelhaf, G. Stiller, M. Kaufmann, M.E. Koukouli, J.-M. Flaud, C. R. Physique 6 (2005) 848.
[7] J.-M. Flaud, C. Camy-Peyret, A. Barbe, C. Secroun, P. Jouve, J. Mol. Spectrosc. 80 (1980) 185.
[8] C. Camy-Peyret, J.-M. Flaud, M.A.H. Smith, C.P. Rinsland, V. Malathy Devi, J.J. Plateaux, A. Barbe, J. Mol. Spectrosc. 141 (1990) 134.
[9] J.-M. Flaud, C. Camy-Peyret, C.P. Rinsland, M.A.H. Smith, V. Malathy Devi, Atlas of ozone line parameters from microwave to medium infrared, Academic Press, Boston, 1990.
[10] A. Barbe, S.N. Mikhailenko, Vl.G. Tyuterev, A. Hamdouni, J.J. Plateaux, J. Mol. Spectrosc. 171 (1995) 583.
[11] S.N. Mikhailenko, A. Barbe, Vl.G. Tyuterev, L. Régalia, J.J. Plateaux, J. Mol. Spectrosc. 180 (1996) 227.
[12] A. Barbe, J.J. Plateaux, S.N. Mikhailenko, Vl.G. Tyuterev, J. Mol. Spectrosc. 185 (1997) 408.
[13] A. Barbe, A. Chichery, Vl.G. Tyuterev, S.A. Tashkun, S.N. Mikhailenko, J. Phys. B: 31 (1998) 2559.

[14] J.I. Steinfeld, S.M. Adler-Golden, J.W. Gallagher, J. Phys. Chem. Ref. Data 16 (1987) 911.
[15] J.-M. Flaud, R. Bacis, Spectrochim. Acta A 54 (1998) 3.
[16] S.N. Mikhailenko, A. Barbe, Vl.G. Tyuterev, A. Chichery, Atmos. Ocean. Opt. 12 (1999) 771.
[17] C.P. Rinsland, J.-M. Flaud, A. Perrin, M. Birk, G. Wagner, A. Goldman, A. Barbe, M.R. De Backer-Barilly, S.N. Mikhailenko, Vl.G. Tyuterev, M.A.H. Smith, V. Malathy Devi, D.C. Benner, F. Schreier, K.V. Chance, J. Orphal, T.M. Stephen, JQSRT 82 (2003) 207.
[18] C. Camy-Peyret, J.-M. Flaud, A. Perrin, V. Malathy Devi, C.P. Rinsland, M.A.H. Smith, J. Mol. Spectrosc. 118 (1986) 345.
[19] A. Perrin, A.M. Vasserot, J.-M. Flaud, C. Camy-Peyret, C.P. Rinsland, M.A.H. Smith, V. Malathy Devi, J. Mol. Spectrosc. 143 (1990) 311.
[20] D. Consalvo, A. Perrin, J.-M. Flaud, C. Camy-Peyret, A. Valentin, Ch. Chardonnet, J. Mol. Spectrosc. 168 (1994) 92.
[21] A. Chichery, A. Barbe, Vl.G. Tyuterev, M.-T. Bourgeois, J. Mol. Spectrosc. 206 (2001) 1.
[22] A. Chichery, A. Barbe, Vl.G. Tyuterev, J. Mol. Spectrosc. 206 (2001) 14.
[23] M.-R. De Backer-Barilly, A. Barbe, Vl.G. Tyuterev, Atmos. Ocean. Opt. 16 (2003) 183.
[24] M.-R. De Backer-Barilly, A. Barbe, Vl.G. Tyuterev, M.-T. Bourgeois, J. Mol. Spectrosc. 221 (2003) 174.
[25] A. Chichery, A. Barbe, Vl.G. Tyuterev, S.A. Tashkun, J. Mol. Spectrosc. 205 (2001) 347.
[26] A. Barbe, M.-R. De Backer-Barilly, Vl.G. Tyuterev, S.A. Tashkun, Appl. Opt. 42 (2003) 5136.
[27] S.N. Mikhailenko, Yu. Babikov, Vl.G. Tyuterev, A. Barbe, Comp. Technologies 7 (2002) 64, (in Russian).
[28] H. Wenz, W. Demtroder, J.-M. Flaud, J. Mol. Spectrosc. 209 (2001) 267.
[29] M.-R. De Backer-Barilly, A. Barbe, Vl.G. Tyuterev, D. Romanini, B. Moeskops, A. Campargue, J. Mol. Struct. 780-781 (2006) 225.
[30] A. Campargue, S. Kassi, D. Romanini, A. Barbe, M.-R. De Backer-Barilly, Vl.G. Tyuterev, J. Mol. Spectrosc. 240 (2006) 1.
[31] A. Barbe, M.-R. De Backer-Barilly, Vl.G. Tyuterev, A. Campargue, D. Romanini, S. Kassi, J. Mol. Spectrosc. 242 (2007) 156.
[32] S. Kassi, A. Campargue, M.-R. De Backer-Barilly, A. Barbe, J. Mol. Spectrosc. 244 (2007) 122.
[33] A. Barbe, M.-R. De Backer-Barilly, Vl.G. Tyuterev, S. Kassi, A. Campargue, J. Mol. Spectrosc. 246 (2007) 22.
[34] A. Campargue, M.-R. De Backer-Barilly, A. Barbe, Vl.G. Tyuterev, S. Kassi, Phys. Chem. Chem. Phys. 10 (2008) 2925.
[35] J.Zúñiga, J. A.G. Picón, A.Bastida, and A.Requena, J. Chem. Phys. **126**, (2008) 1244305
[36] R. Siebert, P. Fleurat-Lessard, R. Schinke, M. Bittererova, M.S.C. Farantos, J. Chem. Phys. 116 (2002) 9749.
[37] R. Schinke, P. Fleurat-Lessard. J. Chem. Phys. 121 (2004) 5789.
[38] D. Babikov, B.K. Kendrick, R.B. Walker, R.T Pack, P. Fleurat-Lesard, R. Schinke, J. Chem. Phys. 118 (2003) 2577.
[39] S.Yu. Grebenshchikov, R. Schinke, P. Fleurat-Lessard, M. Joyeux, J. Chem. Phys. 119 (2003) 6512.
[40] Vl.G. Tyuterev, S.A. Tashkun, P. Jensen, A. Barbe, T. Cours, J.Mol. Spectrosc. 198 (1999) 57.
[41] Vl.G. Tyuterev, S.A. Tashkun, D.W. Schwenke, P. Jensen, T. Cours, A. Barbe, M. Jacon, Chem. Phys. Lett. 316 (2000) 271.
[42] Vl.G. Tyuterev, S.A. Tashkun, H. Seghir, SPIE Proc. Ser. 5311 (2004) 164.

[43] J. Lamouroux, S.A. Tashkun, Vl.G. Tyuterev, Chem. Phys. Lett. 452 (2008) 225.
[44] J. Morville, D. Romanini, A.A. Kachanov, M. Chenevier, Appl. Phys. D78 (2004) 465.
[45] P. Macko, D. Romanini, S.N. Mikhailenko, O.V. Naumenko, S. Kassi, A. Jenouvrier, Vl.G. Tyuterev, J. Mol. Spectrosc. 227 (2004) 90.
[46] S. N. Mikhailenko, W. Le, S. Kassi and A. Campargue, J. Mol. Spectrosc. 244 (2007) 170.
[47] B.V. Perevalov, S. Kassi, D. Romanini, V.I. Perevalov, S.A. Tashkun, A. Campargue, J. Mol. Spectrosc. 238 (2006) 241.
[48] B.V. Perevalov, S. Kassi, V.I. Perevalov, S.A. Tashkun, A. Campargue, J. Mol. Spectrosc. (in press) doi: 10.1016/j.jms.2008.06.012
[49] L.S. Rothman, D. Jacquemart, A. Barbe, D. Chris Benner, M. Birk, L.R. Brown,M.R. Carleer, C. Chackerian, Jr, K. Chance, V. Dana, V.M. Devi, J.-M. Flaud, R.R.Gamache, A. Goldman, J.-M. Hartmann, K.W. Jucks, A.G. Maki, J. Y. Mandin, S.T.Massie, J. Orphal, A. Perrin, C.P. Rinsland, M.A.H. Smith, J. Tennyson, R.N.Tolchenov, R.A. Toth, J. Vander Auwera, P. Varanasi, G. Wagner, JQSRT 96 (2005) 139.
[50] M.Kellmann, J.Chem.Phys. 83 (1985) 3843.

Figure Captions

Figure 1:
Overview of the CW-CRDS spectrum of $^{18}O_3$ between 5925 and 6850 cm^{-1}. The $^{18}O_3$ sample pressure was about 18 Torr. The displayed spectrum was obtained by concatenating 39 individual spectra recorded successively with different DFB laser sources (the corresponding ranges are shown with different colors / grey levels). The CW-CRDS spectrum is observed above the baseline fixed by the reflectivity of the used super mirrors. The A-type parallel bands are indicated and assigned with the usual normal mode label. Note the rapid decrease of their band strength with the energy. The stronger absorption bands due to impurities (CO_2 and H_2O) are also indicated.

Figure 2:
Comparison of the simulated spectra using assigned ro-vibrational lines for $^{18}O_3$ (upper panel) and $^{16}O_3$ (lower panel) in the region of the $5\nu_1+\nu_3$ bands. The global and normal mode band assignments are shown. The vertical axe represents the absorption coefficient in arbitrary units at the same scale for both isotopologues.

Figure 3:
Isotopic shift due to the $^{16}O_3 \rightarrow {}^{18}O_3$ homogeneous isotopic substitution for the centers of the $^{18}O_3$ bands observed by CW-CRDS between 5900 and 6850 cm^{-1}.
Upper panel (diamonds): wavenumber difference between the band centres having the same global assignment; *Lower panel* (circles): wavenumber difference between the centers of bands associated with the most similar compositions of the normal mode upper states.
See text of the Section 5 explaining the distinctions between filled, grey and open symbols.

Figure 4.
Principal normal mode mixing coefficients for upper vibration states involved in Fig 3.
Upper panel: $^{18}O_3$ states observed in this work. *Lower panel:* corresponding $^{16}O_3$ states (lower panel of Figure 3).
The vertical axe represents the mixing coefficients P_1 for the normal mode expansion of the wavefunctions, Eqs. (1,2). Triangles correspond to ψ for the $[JK_aK_c]=[0\ 0\ 0]$ level of A_1 vibration states. Stars correspond to ψ for the lowest possible $[JK_aK_c]=[1\ 0\ 1]$ level of B_1 vibration states.

Table 1

Theoretical prediction of the lowest rovibrational levels of excited states corresponding to the observed bands of $^{18}O_3$ and their global and normal mode assignment

N_V	E / hc [cm^{-1}] Calc_1	Calc_2	$J\ K_a\ K_c$	P_1(%) W_1	P_2(%) W_2	P_3(%) W_3
			A_1 vibration states			
65	6012.31	6011.74	0 0 0	72 $(430)_o$	10 $(322)_o$	9 $(124)_o$
66	6047.95	6046.71	0 0 0	41 $(214)_o$	17 $(124)_o$	14 $(412)_o$
71	6245.81	6245.50	0 0 0	49 $(016)_o$	23 $(304)_o$	10 $(106)_o$
82	6591.83	6592.73	0 0 0	32 $(134)_o$	26 $(224)_o$	11 $(422)_o$
			B_1 vibration states (A_2 ro-vibrational symmetry)			
44	5985.28	5985.58	1 0 1	49 $(025)_o$	10 $(223)_o$	10 $(313)_o$
45	6013.84	6013.71	1 0 1	74 $(501)_o$	22 $(303)_o$	3 $(105)_o$
46	6073.20	6071.34	1 0 1	28 $(115)_o$	27 $(313)_o$	23 $(223)_o$
51	6272.97	6271.24	1 0 1	44 $(205)_o$	28 $(403)_o$	12 $(115)_o$
54	6394.42	6394.58	1 0 1	38 $(233)_o$	23 $(143)_o$	11 $(035)_o$
58	6558.19	6560.01	1 0 1	37 $(035)_o$	13 $(323)_o$	12 $(125)_o$
59	6611.19	6610.71	1 0 1	69 $(511)_o$	16 $(313)_o$	6 $(007)_o$
60	6644.93	6642.85	1 0 1	35 $(233)_o$	12 $(323)_o$	10 $(431)_o$
64	6796.01	6797.32	1 0 1	38 $(125)_o$	16 $(413)_o$	15 $(215)_o$
66	6828.44	6826.45	1 0 1	38 $(431)_o$	20 $(323)_o$	11 $(233)_o$

N_V : global ranking number for A_1 and B_1 vibrational states. Calc_1: variational predictions from the PES V^M of Ref. [40] in internal coordinates (r_1, r_2, θ); Calc_2: non-empirical effective Hamiltonian predictions derived from the PES of Ref. [41] in normal coordinates q_1, q_2, q_3 using 8-th order Contact Transformations [42]; $J\ K_a\ K_c$: rotational quantum numbers; Columns P_1, P_2, P_3 indicate the first three mixing coefficients (in %) according to Eqs. (1,2); Columns W_1, W_2, W_3 indicate the corresponding vibration normal mode quantum numbers ($\upsilon_1 \upsilon_2 \upsilon_3$). The subscript "0" of ($\upsilon_1 \upsilon_2 \upsilon_3$) $_0$ means that these contributions correspond to the harmonic normal mode basis.

Table 2

Bands of $^{18}O_3$ analysed in the CW-CRDS spectrum between 5900 and 7000 cm^{-1} and comparison with the calculations from the PES

Observed bands: spectroscopic notations	Normal mode assignment of the upper vibration state	Global band assignment	Number of assigned ro-vib. lines	Band centres σ			
				σ(exp.) (cm^{-1})	dσ (10^{-3} cm^{-1})	Calc_1 (cm^{-1})	obs-calc (cm^{-1})
			B-type bands				
$4\nu_1 + 3\nu_2$	(430)	65A ← 1A	32	6011.836	9	6012.31	-0.5
$2\nu_1 + \nu_2 + 4\nu_3$	(214)	66A ← 1A	184	6047.101	14	6047.95	-0.8
$\nu_2 + 6\nu_3$	(016)	71A ← 1A	91	6245.039	11	6245.81	-0.7
$\nu_1 + 3\nu_2 + 4\nu_3$	(134/224)	82A ← 1A	339	6592.661	14	6591.83	0.9
			A-type bands				
$2\nu_2 + 5\nu_3$	(025)	44B ← 1A	507	5984.439	6	5984.58	-0.1
$5\nu_1 + \nu_3$	(501)	45B ← 1A	567	6013.048	8	6013.12	-0.1
$\nu_1 + \nu_2 + 5\nu_3$	(115/313/223)	46B ← 1A	599	6072.132	6	6072.49	-0.4
$2\nu_1 + 5\nu_3$	(205/403)	51B ← 1A	659	6270.604	7	6272.27	-1.7
$2\nu_1 + 3\nu_2 + 3\nu_3$ (I)	(233/143)	54B ← 1A	344	6392.214	9	6393.72	-1.5
$3\nu_2 + 5\nu_3$	(035)	58B ← 1A	574	6556.788	2	6557.49	-0.7
$5\nu_1 + \nu_2 + \nu_3$	(511)	59B ← 1A	254	6611.039	34	6610.48	0.6
$2\nu_1 + 3\nu_2 + 3\nu_3$ (II)	(233/323)	60B ← 1A	355	6642.896	21	6644.23	-1.3
$\nu_1 + 2\nu_2 + 5\nu_3$	(125/413/215)	64B ← 1A	385	6796.463	6	6795.31	1.2
$4\nu_1 + 3\nu_2 + \nu_3$	(431/323)	66B ← 1A	165	6825.512	6	6827.74	-2.2

In case of a large normal mode mixing of the upper states, several contributions are given in column 2 according to Table 1. Column 3 represents the global unambiguous assignment (see text), dσ is the uncertainty estimation for the experimental band centre determination. The bands at 6392 and 6643 cm^{-1} have the same principal normal mode contributions (Table 1) for the upper states.

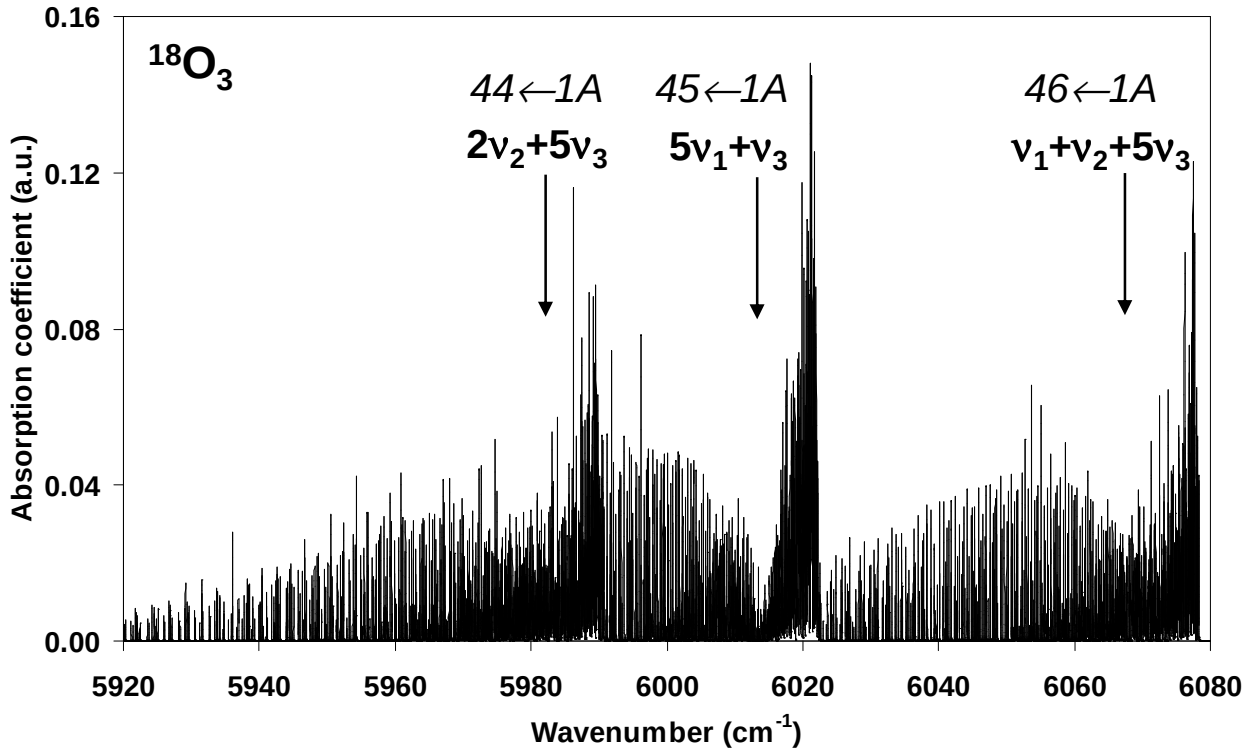
$^{18}O_3$
44←1A
$2\nu_2+5\nu_3$
45←1A
$5\nu_1+\nu_3$
46←1A
$\nu_1+\nu_2+5\nu_3$
Absorption coefficient (a.u.)
0.16
0.12
0.08
0.04
0.00
5920
5940
5960
5980
6000
6020
6040
6060
6080
Wavenumber (cm^{-1})

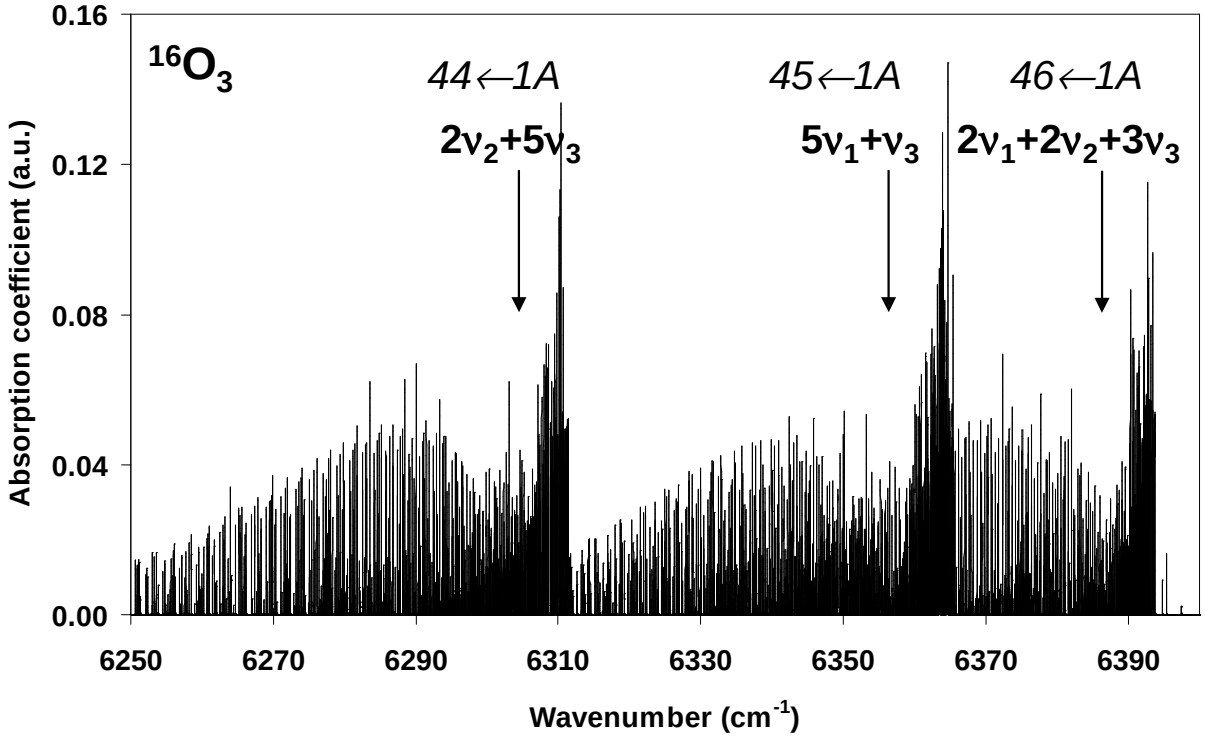
$^{16}O_3$
44←1A
$2\nu_2+5\nu_3$
45←1A
$5\nu_1+\nu_3$
46←1A
$2\nu_1+2\nu_2+3\nu_3$
Absorption coefficient (a.u.)
0.16
0.12
0.08
0.04
0.00
6250
6270
6290
6310
6330
6350
6370
6390
Wavenumber (cm^{-1})

Figure 3

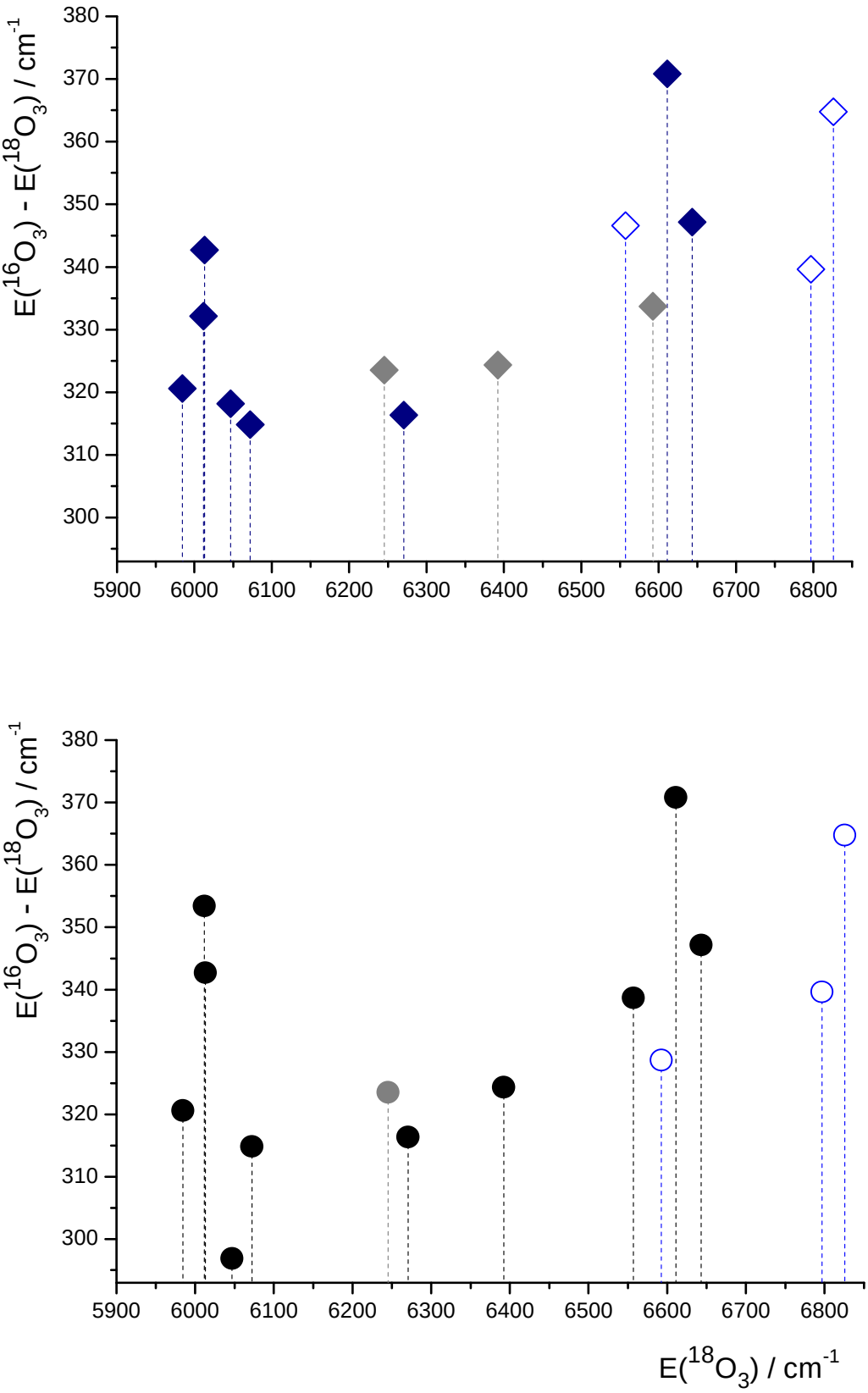
E(16O3) - E(18O3) / cm-1
380
370
360
350
340
330
320
310
300
5900
6000
6100
6200
6300
6400
6500
6600
6700
6800
E(18O3) / cm-1

Figure 4

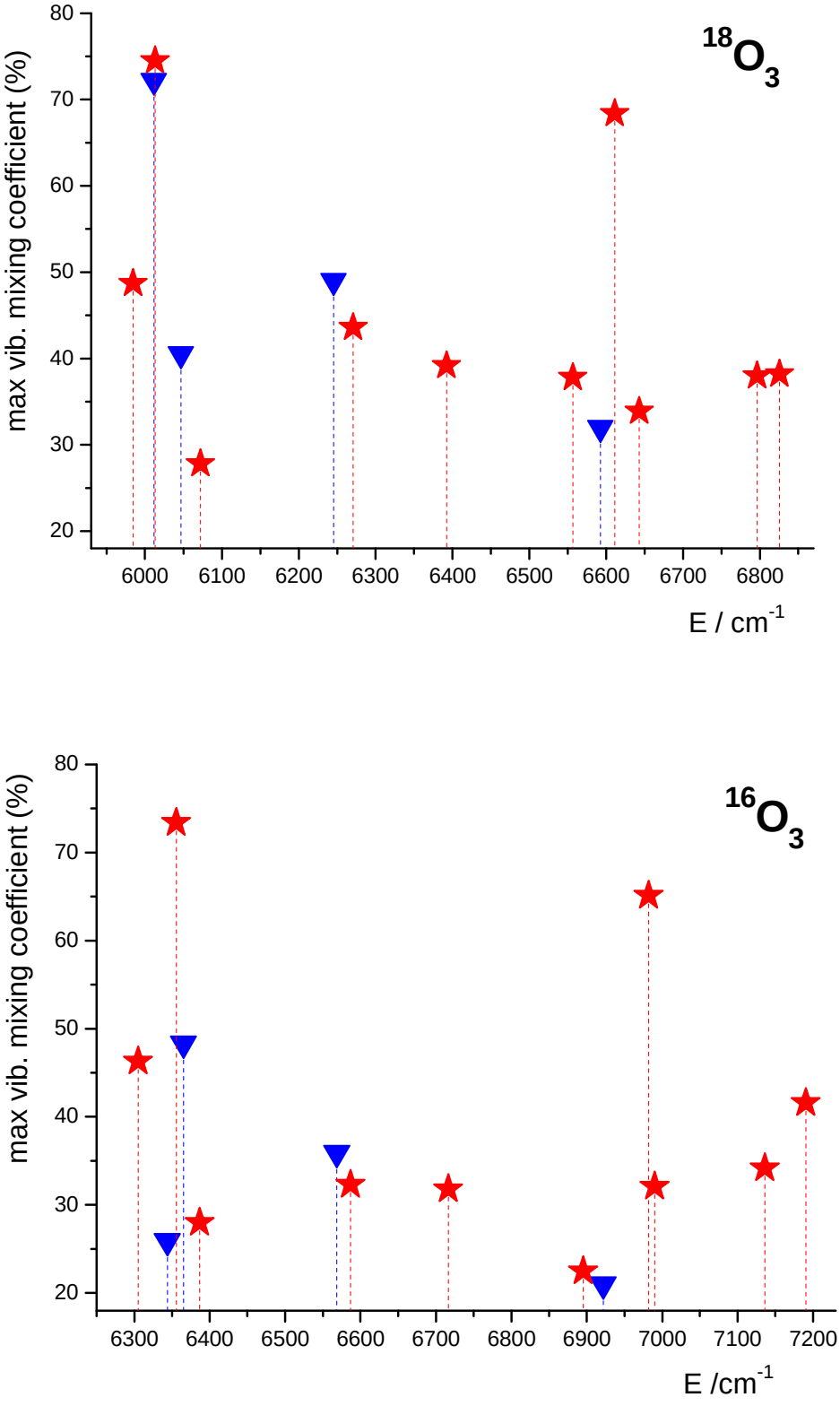
$^{18}O_3$
max vib. mixing coefficient (%)
80
70
60
50
40
30
20
6000
6100
6200
6300
6400
6500
6600
6700
6800
E / cm^{-1}
$^{16}O_3$
max vib. mixing coefficient (%)
80
70
60
50
40
30
20
6300
6400
6500
6600
6700
6800
6900
7000
7100
7200
E /cm^{-1}